Correlating nano-scale surface replication accuracy and cavity temperature in micro-injection moulding using in-line process control and high-speed thermal imaging

Baruffi, Federico; Gulcur, Mert; Calaon, Matteo; Romano, Jean-Michel; Penchev, Pavel; Dimov, Stefan; Whiteside, Ben ; Tosello, Guido

DOI:
10.1016/j.jmapro.2019.08.017
10.1016/j.jmapro.2019.08.017

Document Version
Peer reviewed version

Citation for published version (Harvard):
Baruffi, F, Gulcur, M, Calaon, M, Romano, J-M, Penchev, P, Dimov, S, Whiteside, B & Tosello, G 2019, 'Correlating nano-scale surface replication accuracy and cavity temperature in micro-injection moulding using in-line process control and high-speed thermal imaging', *Journal of Manufacturing Processes*, vol. 47, pp. 367-381. https://doi.org/10.1016/j.jmapro.2019.08.017, https://doi.org/10.1016/j.jmapro.2019.08.017

Correlating nano-scale surface replication accuracy and cavity temperature in micro-injection moulding using in-line process control and high-speed thermal imaging

Federico Baruffi[a,*], Mert Gülçür[b], Matteo Calaon[a], Jean-Michel Romano[c], Pavel Penchev[c], Stefan Dimov[c], Ben Whiteside[b], Guido Tosello[a]

[a] Department of Mechanical Engineering, Technical University of Denmark, Building 427A, DK-2800 Kgs. Lyngby, Denmark

[b] Centre for Polymer Micro & Nano Technology, School of Engineering, University of Bradford, Tumbling Hill St., Bradford, BD7 1DP, UK

[c] Department of Mechanical Engineering, School of Engineering, University of Birmingham, 142 Edgbaston Park Rd, Birmingham, B15 2TT, UK

*Corresponding author. Tel.: +45 45 25 48 22; Fax: +45 45 25 19 61

E-mail address: febaru@mek.dtu.dk (Federico Baruffi)

Keywords: Micro-injection moulding, Flow visualization, Surface replication, In-line quality assurance

ABSTRACT

Micro-injection moulding (µIM) stands out as preferable technology to enable the mass production of polymeric components with micro- and nano-structured surfaces. One of the major challenges of these processes is related to the quality assurance of the manufactured surfaces: the time needed to perform accurate 3D surface acquisitions is typically much longer than a single moulding cycle, thus making impossible to integrate in-line measurements in the process chain. In this work, the authors proposed a novel solution to this problem by defining a process monitoring strategy aiming at linking sensitive in-line monitored process variables with the replication quality. A nano-structured surface for antibacterial applications was manufactured on a metal insert by laser structuring and replicated using two different polymers, polyoxymethylene (POM) and polycarbonate (PC). The replication accuracy was determined using a laser scanning confocal microscope and its dependence on the variation of the main

µIM parameters was studied using a Design of Experiments (DoE) experimental approach. During each process cycle, the temperature distribution of the polymer inside the cavity was measured using a high-speed infrared camera by means of a sapphire window mounted in the movable plate of the mould. The temperature measurements showed a high level of correlation with the replication performance of the µIM process, thus providing a fast and effective way to control the quality of the moulded surfaces in-line.

1. Introduction

In the recent decade, micro- and nano-structured surfaces have attracted great attention in many fields such as microfluidics [1] and optics [2]. The most efficient and cost-effective way to manufacture components featuring this type of surfaces is to replicate a master geometry using a polymeric material [3]. Many technologies can serve this purpose: among them, micro-injection moulding (µIM) stands out as the preferable one because of its high replication accuracy and short cycle times [4]. In this process, plastic granules are melted and then injected at high speed and temperature inside a mould cavity having the negative shape of the final part. The accuracy of the mould features is essential to guarantee the outcome of µIM, and thus tooling processes such as electron beam lithography [5], photolithography [6] and laser machining [7] are typically employed to fabricate the structured inserts.

The replication of micro- and nano-structured surfaces is challenging, particularly when high aspect-ratio features are the target [8] since the injected polymer flow tends to solidify at the entrance of the micro features (hesitation effect) [9]. Adopting a state-of-the-art µIM machine having separate plasticizing screw and injection plunger can substantially improve the capability of the moulding process, but the complete replication of the mould features is still difficult to achieve.

In order to tackle this issue, various approaches have been proposed by researchers. Mould temperature and injection speed were reported as key factors when filling micro cavities [10]: high levels of these process parameters oppose the premature solidification of the polymer melt caused by the large surface-to-volume ratio of micro components. A high mould temperature is needed to maximize replication of micro and nano features since it also contrasts the growth of

the frozen layer [11]. With this aim, rapid heat cycle technologies were developed in order to maintain a high mould temperature during the filling and, at the same time, increasing the cooling rate after the completion of the holding phase to keep the throughput rate at acceptable levels for industrial purposes [12,13].

Since the effects of µIM process parameters on the replication fidelity are very significant, the process optimization phase becomes central for obtaining a product that complies with the design specifications. Many authors studied the effects of different process parameters on the replication level by applying statistical methods such as Design of Experiments (DoE) [14–16]. To do this, a comparison between the mould and the moulded parts, based on an accurate measurement of the surface texture, must be carried out. Optical instruments are preferable for this task since they provide a three-dimensional map of the surface, feature sub-micrometric resolutions and do not risk damaging the sample because of their contact-less nature [17]. However, the high throughput rate of µIM does not allow to assess the quality of all the manufactured polymeric parts using an in-line approach, being the measuring time of typical optical instruments much longer than a single moulding cycle. Therefore, the production quality is usually verified by assessing a few components randomly extracted by the produced batch. The most promising solution for in-line characterization of injection moulded samples having structured surfaces is nowadays scatterometry [18], which however is best suited for well-defined micro and nano structures such as gratings and therefore cannot be successfully applied to more complex and irregular surfaces such as laser textured ones.

The adoption of a strategy based on process monitoring can prove very useful in tackling this issue. By linking variables, referred to as “process fingerprints”, that are monitored for each moulding cycle, to the replication level of each manufactured part, a strategy aiming at implementing an in-line quality control can be defined [19], making the process optimization phase much faster without losing accuracy. An effective process fingerprint must be correlated to the quality of the replicated surface as well as sensible to process parameter variations in order to function as an optimization tool for the µIM process. Therefore, by controlling the values of this indicator, the quality of the produced parts can be assessed within the production chain without performing any off-line measurement procedure.

Process monitoring of injection moulding technologies has been often reported in the literature. In most studies [20–23], pressure and temperatures sensors were placed inside the cavity to study the filling of the cavity during the whole moulding cycle. The information derived by this type of transducers allows detailed evaluation of real processing conditions [24], which can differ from the ones set by the user at the machine interface. Moreover, constant monitoring of the µIM variables is fundamental since small variations of the material properties can have a significant effect on the final part characteristics.

Another typology of process monitoring technique that can be applied to injection moulding is flow visualization. This method is based on the use of a high-speed camera capable of recording the advancement of the polymer flow inside the cavity at high frame rates [25]. To do this, the mould must have a lateral opening and one side of the cavity made of glass in order to allow the camera access. This technique is particularly useful since it allows to actually observe the evolution of the filling and, if an infrared camera is used, to gather temperature data in the whole cavity and not just in one point as it is when measuring with a thermocouple. In µIM literature, flow visualization in has been reported as a powerful tool for filling analysis [26], process characterization [27], heat transfer determination [28] and validation of moulding simulations [29]. However, the applicability of flow visualization as a monitoring tool for the assurance of surface replication has not been investigated yet. By correlating variables monitored with flow visualization to the replication level of the µIM process, an in-line quality assurance strategy based on high-speed camera acquisitions can be designed to control the quality of all the produced parts. By achieving this, the off-line measurement phase can be eliminated and, consequently, the process optimization phase significantly shortened.

The present paper introduces a study aimed at investigating the use of flow visualization as a tool for predicting the quality of nano-structured surfaces for biomedical applications replicated by µIM using polyoxymethylene (POM) and polycarbonate (PC). An experimental DoE approach was implemented to evaluate the effects of the main µIM process parameters on both surface replication and in-cavity temperature profiles recorded with a high-speed infrared camera. A correlation study was performed to identify the process fingerprint that allowed the most accurate prediction on the replication level, thus providing useful insights on how to control the outcome of the process in-line.

2. Materials and methods

2.1 Case study and mould design

The moulded part was a disc with diameter 17.0 mm and thickness 0.6 mm (total volume of circa 135 mm^3) featuring a circular nano-structured area of diameter 10 mm that serves for antibacterial purposes. This area was manufactured by replicating a laser-structured insert made of tool steel integrated into a Hasco-K standard modular system with a single cavity (see Fig. 1).

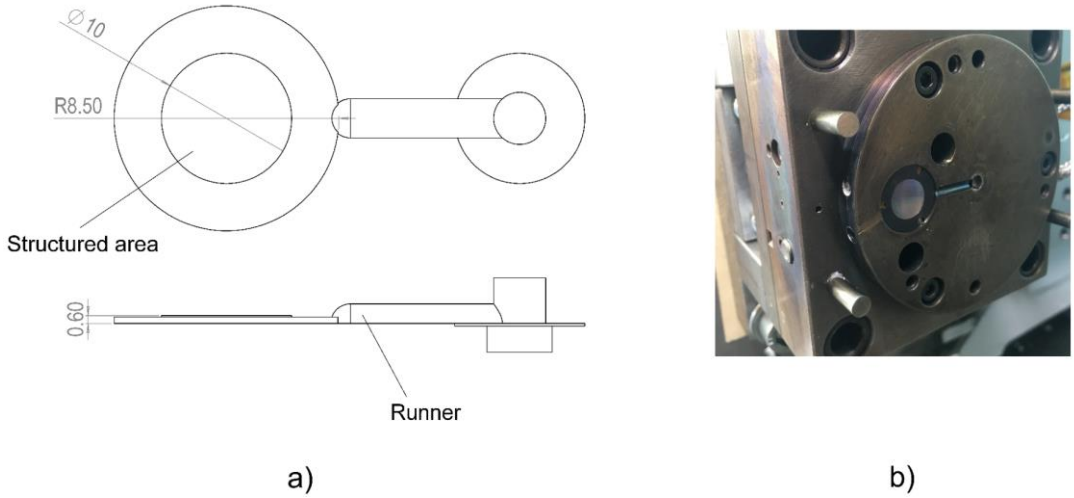

Fig. 1. a) Geometry and nominal dimensions in mm of the moulded part. b) Movable side of the mould with nano-structured insert.

In particular, a Yb-doped sub-pico 5 W laser source by Amplitude Systemes operating on a wavelength of 1030 nm was used. An average laser power of 0.55 W, a scanning speed of 2 m/s and a frequency of 500 kHz were the parameters selected to generate the surface. The resulting texture presented a single-lay periodic pattern. The average height of the ripples generated on the insert was 50 nm while the pitch 900 nm (see Fig. 2).

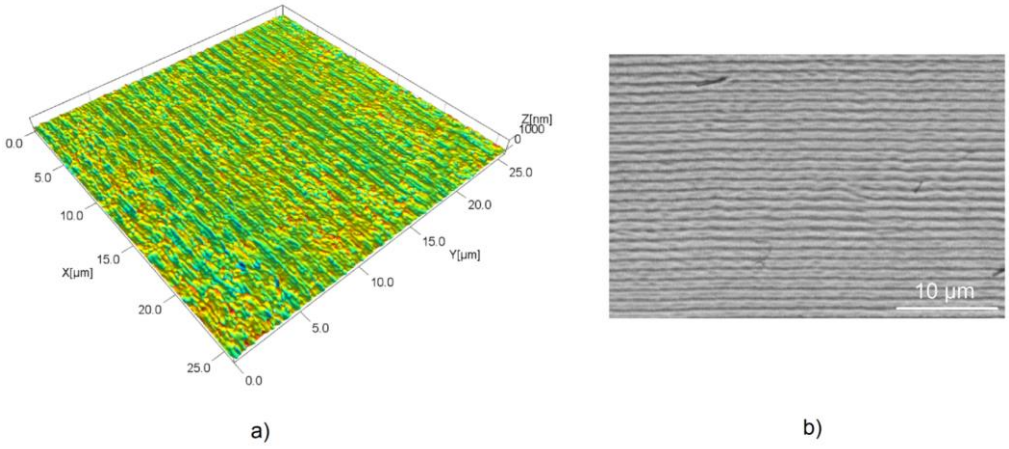

Fig. 2. Appearance of the laser-textured surface of the insert: a) 3D acquisition with confocal microscope, b) SEM image.

The mould was modified to integrate a 45° tilted mirror and a sapphire window in the movable plate in order to allow the visualization of the cavity during moulding (see Fig. 3 a)). A high-speed infrared camera (FLIR X6540 SC) was aligned to the mirror, thus allowing the observation through the sapphire window (see Fig. 3 b)). The camera, which had been previously calibrated over a range of temperature of 55 to 300 °C, had a cooled indium antimonide (InSb) focal plane array detector with a spectral range of 1.5 to 5.0 µm. It was operated with a framerate of 100 Hz and a field of view of 9 mm × 7 mm, which was set to maximum and allowed to cover most of the nano-structured cavity. The distance between the camera objective and the mould lateral opening was defined to image the surface of the nano-structured insert. Therefore, the temperature at the mould-polymer interface, which plays a central role in the replication mechanism of injection moulding processes, was monitored. Each acquisition was triggered manually at the start of the injection cycle. The temperature information for each pixel and time step was then extracted using a dedicated software coupled with the infrared camera.

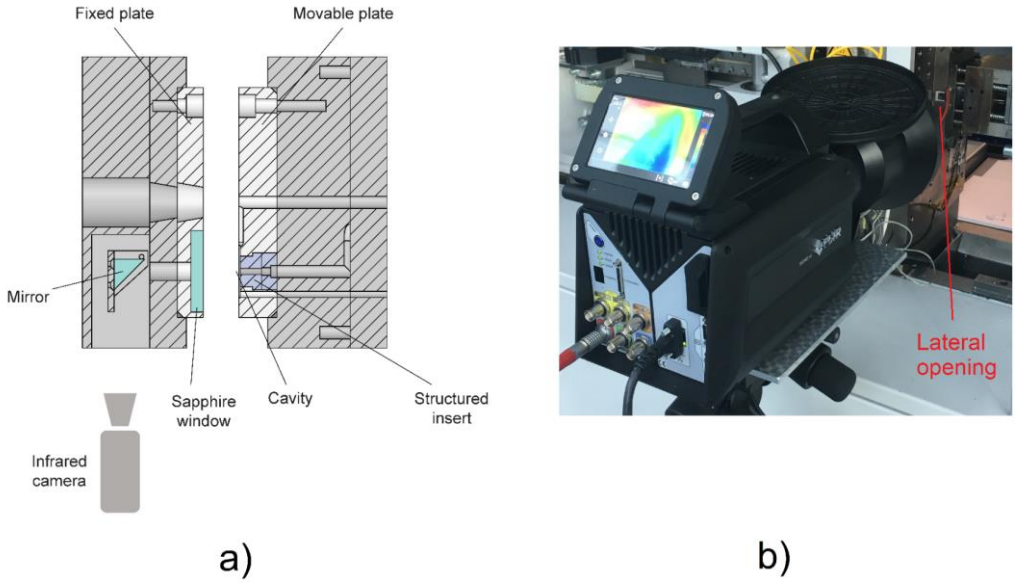

Fig. 3. a) Scheme of the mould system with the flow visualization apparatus. b) Infrared camera imaging the cavity through the sapphire window.

2.2 Experimental details

A state-of-the-art µIM machine (Wittmann Battenfeld MicroPower 15) was used for the moulding experiments. This machine has a plasticizing screw of diameter 14 mm for melting and homogenising the material and an injection plunger of diameter 5 mm to drive the melt inside

the cavity. Two different polymers were used in the experiments: unfilled polyoxymethylene (Hostaform® C27021, manufactured by Celanese) and polycarbonate (Makrolon® AL2447, manufactured by Covestro). Table 1 reports the main characteristics of the two polymer grades and Fig. 4 shows their viscosity data.

Table 1 Main properties of the two moulded materials.

Polymer	Density/(kg/m^3)	Melt volume rate/(cm^3/10min)
POM	1410	24
PC	1200	19

The two materials have high flowability as indicated by their very high melt volume rate (MVR) values and, thus, are suitable for filling small details such as the nano structures of the insert. In particular, the two polymers were selected since they exhibited very similar viscosity values at the experimented conditions (see Fig. 4) even though their molecular structure is different, being POM semi-crystalline and PC amorphous. Therefore, comparing the behaviours of the two materials with respect to the variation of the processing conditions allowed evaluating the influence of the different molecular structure on the replication quality at the nano-scale.

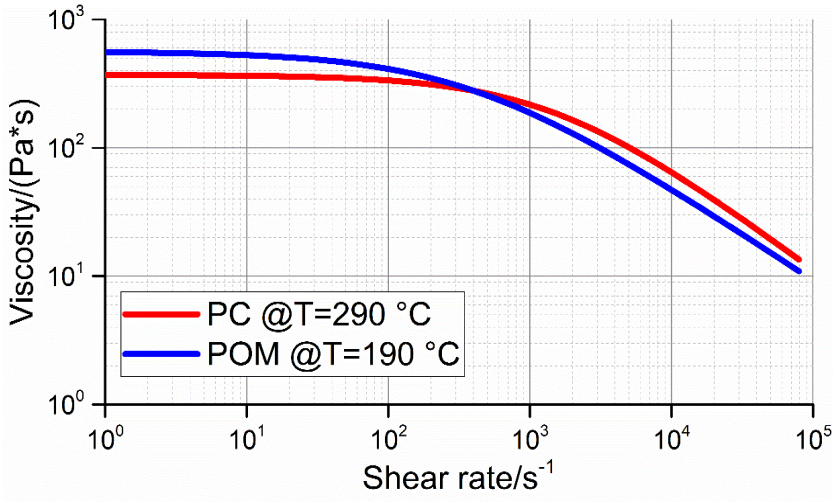

Fig. 4. Viscosity plot at the experimented melt temperatures. Source: Autodesk Moldflow® 2017 material database.

A Design of Experiments (DoE) approach was adopted to study the effects of the variation of the main µIM process parameters on the replication for both polymeric materials. Four process parameters were varied, namely holding pressure, injection speed, mould temperature and melt temperature. These variables were selected since they are widely reported in the literature as being the most influential for the replication of mould features [10,14,30]. A two-level full factorial 2^4 experimental design was carried out, resulting in 16 process setting combinations.

For each experimental run, the first ten moulded parts were discarded and the following five kept for evaluation. Therefore, 80 moulded parts per material were characterized and considered in the analysis. Table 2 shows the levels of the process parameters, which were identified in a preliminary experimentation starting from the manufacturer's recommendations and aiming at obtaining consistent filling and minimized warpage of the moulded disc. In order to evaluate the difference of the two materials in terms of replication performance, they were processed in similar conditions: the same levels of mould temperature and injection speed were selected in the two cases and the same range of variation was also kept for holding pressure and melt temperature settings.

Table 2 DoE process settings for the two materials.

			POM		PC	
Process parameter	Symbol	Unit	Low level	High level	Low level	High level
Holding pressure	p_{hold}	bar	250	750	750	1250
Injection speed	v_{inj}	mm/s	50	150	50	150
Mould temperature	T_{mould}	°C	100	120	100	120
Melt temperature	T_{melt}	°C	190	210	290	310

2.3 Surface topography measurement strategy and uncertainty evaluation

The insert and the replicated polymer surfaces were characterized using a laser scanning confocal microscope (Olympus Lext OLS4100) with a 100× magnification objective lens. The main characteristics of the instrument are reported in Table 3. This measurement solution was particularly suitable for the task since the instrument is capable of acquiring also transparent samples such as those moulded with PC. Moreover, a fine lateral resolution was necessary to characterize the finely-spaced ripples of the laser-structured surface (see Fig. *2*).

Table 3 Laser scanning confocal microscope characteristics.

Instrument characteristic	Value
Objective magnification	100×
Numerical aperture	0.95
Working distance/mm	0.35
Field of view/µm	129 × 129
Digital lateral resolution/µm	0.03
Declared vertical resolution/nm	10

Different areas were acquired on metal insert and moulded parts to evaluate the homogeneity of replication. In fact, it is of primary importance to ensure that the mould nano features were replicated at the same level over the entire structured area. Five measurement areas were defined: one correspondent to the centre of the circular area, two along the flow direction and two on the perpendicular to the flow direction. The distance between the central area and the other ones was 2 mm. By measuring over these areas, the influence of the distance from the gate on the replication accuracy as well as the symmetry of replication could be evaluated. Fig. 5 shows the scheme of the measured areas, which were named according to the Cartesian coordinates of a plane centred on the central area of the nano-structured circle. Each acquisition was repeated three times.

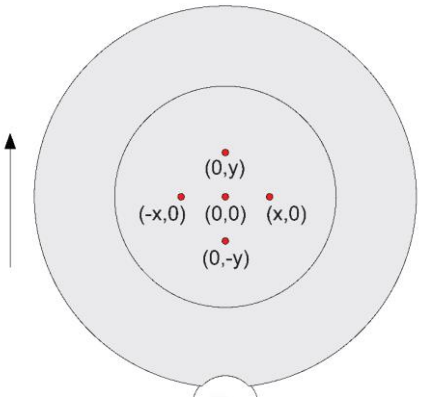

Fig. 5. Measurement areas and their nomenclature. The black arrow represents the flow direction.

The raw acquisitions of the surfaces of both metal insert and moulded parts were post-processed using an image processing software (SPIP 6.7.3, Image Metrology) before extracting quantitative information on the surface texture. Firstly, the 3D acquisitions were flattened by subtracting a first-order plane fitted on the point cloud, thus eliminating any influence of a possible tilt. After that, a spatial filter was applied in order to filter the waviness out, thus evaluating the capability when replicating only the laser-machined ripples. Being the pitch of the ripples circa 900 nm, a linear areal Gaussian high-pass filter [31] at 1.0 µm was applied, thus eliminating the overall waviness of the surface (see Fig. 6). This procedure was necessary because the calculation of surface roughness parameters on the unfiltered surfaces would have been more sensitive to the low-frequency waviness rather than to the texture generated by the nano structures.

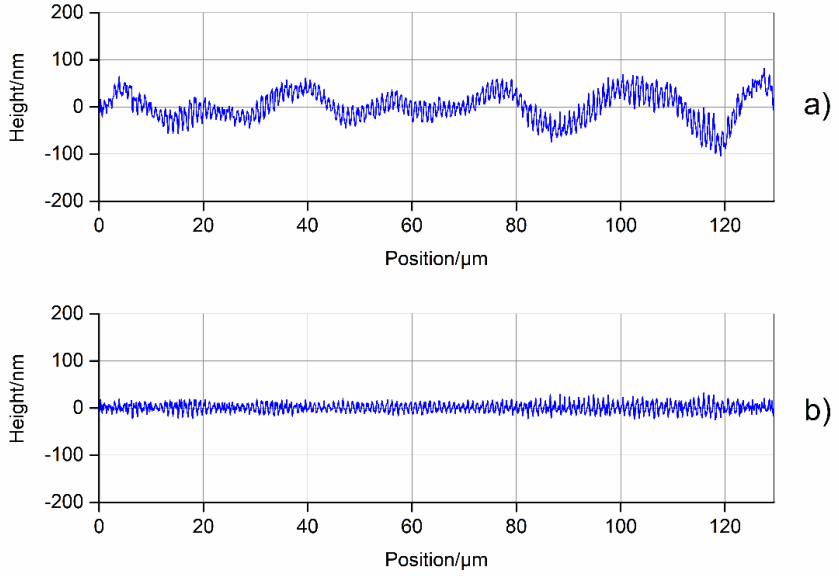

Fig. 6. Average profile of the (0,0) insert surface in the direction perpendicular to the ripples a) before filtering and b) after filtering with a Gaussian high-pass 1.0 µm filter.

After levelling and filtering, the surface topography was evaluated by using areal texture parameters that were then used for assessing the replication by comparing values of master and replicas. In particular, the root mean square of the height *Sq* and the root mean square gradient *Sdq* of the surface were computed [32]. *Sq* provides information on the average areal surface roughness of the surface, thus being a useful indicator for the replication of the height of the laser-machined ripples of the insert. It provides very similar information to the arithmetical mean height *Sa*, which is widely used to characterize antibacterial surfaces [33–35], but it is more sensitive to local spikes or defects due to its quadratic nature. *Sdq* is sensitive to the local slope of the surface and can be used to determine whether local surface slopes have been replicated accurately. Therefore, by calculating *Sq* and *Sdq*, both the height and the slope of the ripples were characterized. Starting from *Sq* and *Sdq* values, two replication indicators were calculated for each of the 80 moulded samples. The indicators were defined as:

$$\Delta_S = \frac{S_{part} - S_{mould}}{S_{mould}} \quad (1)$$

where S_{part} and S_{mould} are *Sq* or *Sdq* calculated for a moulded part and the mould respectively in correspondent measurement areas.

The uncertainty of the surface roughness measurements was also characterized. This procedure was necessary since the variations of replication accuracy due to processing conditions are typically in the order of nanometres when considering surface roughness. Therefore, the precision of the measurement results must be characterized in order to make the

right conclusions on the significance of the effect of a particular process parameter [3]: the uncertainty interval might, in fact, cover the variation induced by the process. In this study, the uncertainty *U* was calculated following ISO 15530-3 [36], which relies on the use of a calibrated artefact to achieve traceability of measurement. In this study, a calibrated injection moulded roughness standard introduced by Tosello et al. [37] and having nominal *Ra* roughness of 100 nm was used. Three uncertainty contributions were taken into account for both *Sq* and *Sdq* measurements: u_{cal}, as the uncertainty of reference AFM measurements on the calibrated artefact [37], u_p, introduced by the measurement procedure and calculated as standard deviation of 20 repeated measurements on the artefact and u_w, associated with material and manufacturing variations of the actual measurand. In this study, u_w was calculated as:

$$u_w = \frac{\max(\boldsymbol{S}) - \min(\boldsymbol{S})}{2\sqrt{3}} \quad (2)$$

where $\boldsymbol{S}$ is the vector listing the three repeated *Sq* or *Sdq* measurements per part. The three contributions were then combined using the law of propagation of uncertainty to determine the expanded uncertainty *U*:

$$U = k \cdot \left(u^2_{cal} + u^2_p + u^2_w\right)^{1/2} \quad (3)$$

where *k* is the coverage factor of 2 selected to achieve a 95 % approximated confidence interval. Table 4 and Table 5 report the uncertainty budgets for *Sq* and *Sdq* measurements of POM and PC moulded parts respectively.

Table 4 Average uncertainty contributions and expanded uncertainty *U* of the measurements of the POM moulded samples.

Uncertainty contribution	*Sq*/nm	*Sdq*
u_{cal}	2.10	0.009
u_p	0.30	0.009
u_w	0.55	0.009
U (*k*=2)	4.4	0.032

Table 5 Average uncertainty contributions and expanded uncertainty *U* of the measurements of the PC moulded samples.

Uncertainty contribution	*Sq*/nm	*Sdq*
u_{cal}	2.10	0.009
u_p	0.30	0.009
u_w	0.26	0.009
U (*k*=2)	4.3	0.032

2.4 Process monitoring strategy

For each moulding cycle, the temperature distribution inside the mould cavity was obtained by processing the videos recorded by the infrared camera using a dedicated software. For PC, the procedure was performed only for the first half of the experimental plan due to feasibility reasons. Therefore, process fingerprint data were analysed according to a 2^3 plan performed at the low melt temperature of 290 °C. Conversely, monitored data derived from the whole 2^4 design were available for POM.

By looking at the recorded infrared images, the behaviour of the polymer melt inside the cavity could be clearly observed. The polymer melt entered the thin cavity and then proceeded to fill it progressively (see Fig. 7 and Fig. 8). Once the filling was complete, the polymer melt started to cool down and the part eventually detached from the sapphire window wall due to volumetric shrinkage. A great influence of the mould temperature can be observed: by comparing Fig. 7 and Fig. 8, it can be seen that when the high level of this parameters was used, the polymer melt not only had a generally higher temperature but also a larger hotter area, indicating that a better adhesion to the sapphire window was also promoted. As a response curve, the curve of the maximum temperature among all the pixels for each time-frame was selected as the output of the process monitoring. In fact, the maximum temperature T_{max} is directly related to the flow front temperature since the pixel having the highest temperature always belonged to the flow front. As such, T_{max} carries valuable information on the polymer melt conditions. This solution also allowed performing a fast and repeatable processing of the infrared videos, as opposed to a procedure based on the evaluation of a portion of the acquired pixels. Therefore, a time-profile of the maximum temperature was extracted for each experimental run.

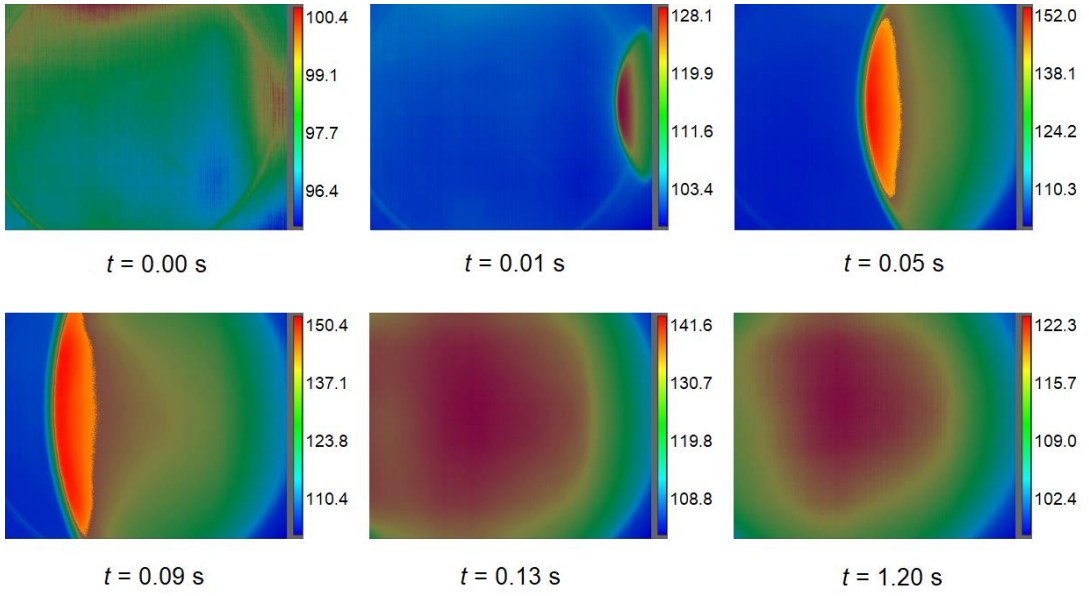

Fig. 7. Infrared images captured at different filling stages during an experiment with POM at low T_{mould}. The circle visible on the background represents the perimeter of the structured area. The contour bars represent the temperature scale in °C.

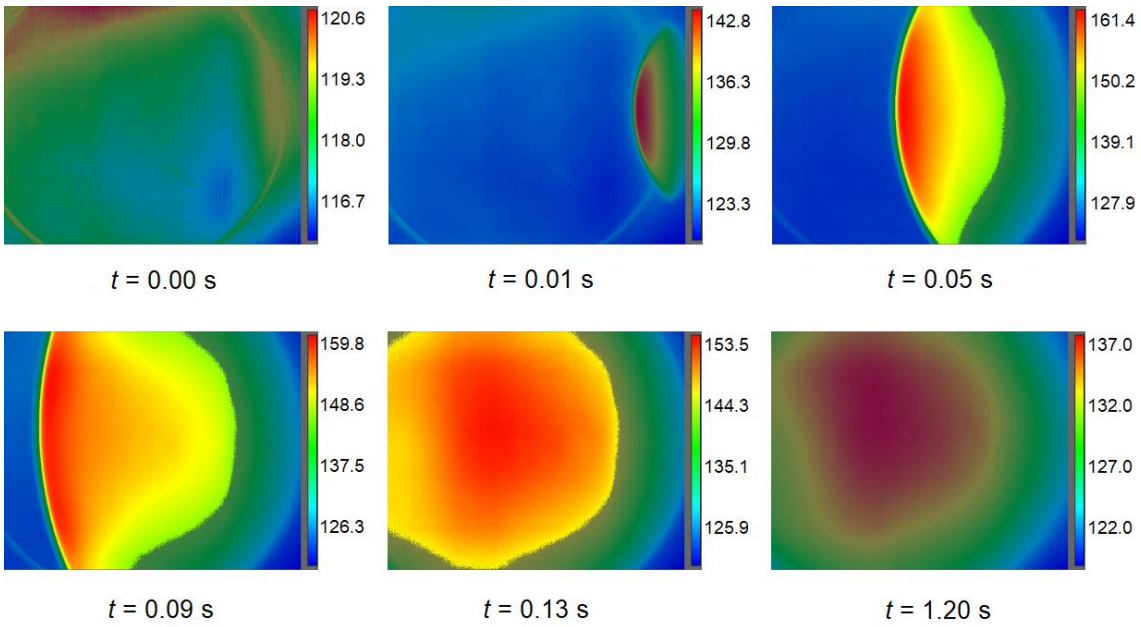

Fig. 8. Infrared images captured at different filling stages during an experiment with POM at high T_{mould}. The circle visible on the background represents the perimeter of the structured area. The contour bars represent the temperature scale in °C.

Fig. 9 shows the shape of five T_{max} profiles correspondent to DoE repetitions. The very high repeatability of the process was reflected by five almost overlapped temperature profiles. After the initial phase in which the temperature equals T_{mould}, a sharp linear increase signalling the start of the filling was observed. Two temperature peaks are distinguishable: the first (T_{peak1}) is related to the burn effect caused by the rapid compression of the air due to the flow front advancement, while the second one (T_{peak2}) represents the maximum flow front temperature

within the cycle [27]. It can be seen that T_{peak2} is lower than the melt temperature: this has been already reported in the literature when using an infrared camera [28] and was caused by the infrared absorption characteristics of POM and PC. In fact, the two materials are selective emitters and appear quite transparent to infrared wavelengths. After the two peaks, the temperature declined rapidly as the polymer melt touched the colder mould surface during the packing and cooling phases of the moulding cycle.

Once the T_{max} profile was extracted for each manufactured part, indicators that well characterized the shape and main features of the curves were calculated and then considered as process fingerprint candidates. Therefore, these variables were investigated with respect to their dependence on process settings variation and to the correlation with the replication quality expressed by Δ_{Sq} and Δ_{Sdq}. In particular, four candidates were identified after a preliminary visual analysis of the curves:

- T_{peak1}: the first temperature peak (see Fig. 9). This quantity relates to the temperature reached at the start of filling due to the burning effect.
- T_{peak2}: the second temperature peak (see Fig. 9), which is related to the maximum flow front temperature reached inside the cavity in the moulding cycle. This variable provides information on the thermal conditions experienced by the polymer melt.
- T_{mean1}: the average temperature in the time interval between point A and B in Fig. 10. It provides average information on the abrupt temperature increase at the beginning of the moulding cycle.
- T_{mean2}: the average temperature in the time interval between point A and C in Fig. 10, which spans from the start of the filling and second peak, thus enclosing the whole filling phase.

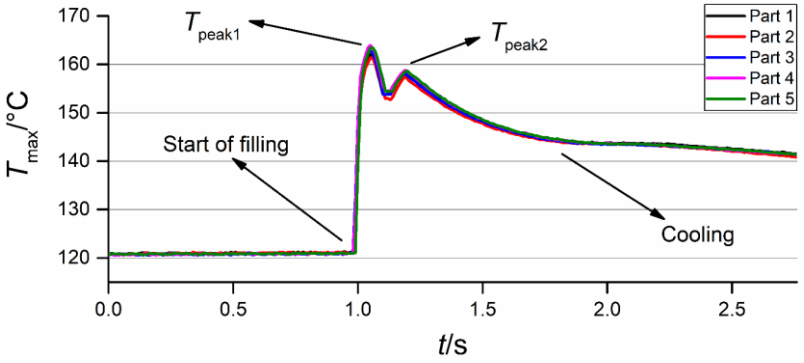

Fig. 9. Maximum temperature profiles during five repeated moulding cycle with POM (T_{mould} = 120 °C, T_{melt} = 190 °C). The moulding phases, as well as the temperature peaks, are indicated.

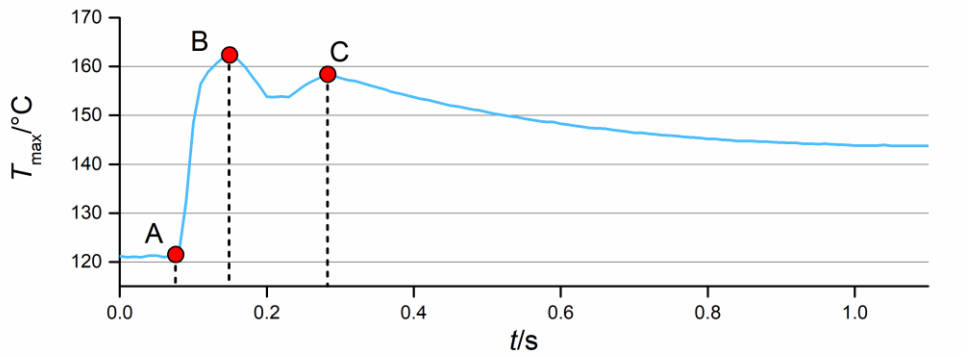

Fig. 10. Maximum temperature curve with points indicating the intervals used for the calculation of the process fingerprint candidates. The points were identified by tracking first-order derivative values.

3. Results and discussion

3.1 Surface replication analysis

The homogeneity of replication among the entire structured area was evaluated by comparing Δ_{Sq} and Δ_{Sdq} values of the five measurement areas. Fig. 11 reports the results for each of the 16 DoE runs. For both POM and PC, the replication quality was congruent throughout the experimental campaign. In fact, no difference was notable between the results of the measurements among the five different positions due to the overlapping of uncertainty intervals. Moreover, the data dispersion for each DoE run was almost constant, proving that also the same level of precision was achieved during the various experiments. Because of this, the results of the five areas were considered as replicates of the DoE plan, thus making 25 replicates available in total considering the five consecutively moulded part per process settings combination. What also stands out in Fig. 11 is the correlation between Δ_{Sq} and Δ_{Sdq} for both materials.

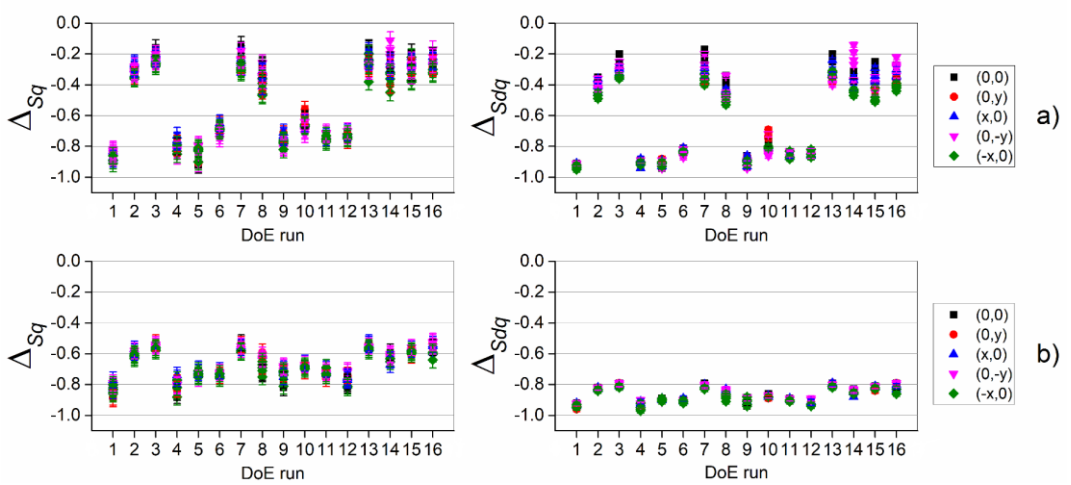

Fig. 11. Replication results for *Sq* and *Sdq* for the five different measurement areas plotted against the 16 DoE runs for a) POM and b) PC. Interval bars represent the expanded measurement uncertainty.

Fig. 12 shows the results of the DoE analysis for POM. Main effects plot and Pareto chart of effects are shown. In the first, the expanded measurement uncertainty *U* is shown to verify whether the measurement precision covered the effect of the process parameters, as it is often the case when dealing with the small dimensional variations typical of micro manufacturing. The replication of both *Sq* and *Sdq* was dominated by the effect of the mould temperature: setting the high T_{mould} resulted in an average increase of circa 0.5 for Δ_{Sq} and Δ_{Sdq}. The positive effect the mould temperature on replication has been already reported in the literature [11,15,38,39] and is related to a decrease of viscosity that in turn facilitates the filling of the surface nano structures. In particular, when using mould temperature of 100 °C, the nano ripples were only partially replicated (see Table 6) as the polymer melt did not fill completely the valleys of the topography of the master surface. This imperfect replication was mirrored in a decay of both *Sq* and *Sdq* since the moulded surface had lower nano structures (i.e. lower *Sq*) and with a generally lower slope (i.e. lower *Sdq*). Conversely, when setting a mould temperature of 120 °C, the replicated features resembled the ones of the insert much more because the local raise of temperature significantly reduced the viscosity of the melt within the nano-structured cavity. The second more relevant process parameter was T_{melt}, whose increase led to a better replication of the master surface. However, considering the measurement uncertainty, this setting cannot be considered as significant since the interval bars of the two levels overlap (see Fig. 12, left). The effects of p_{hold} and v_{inj} can be regarded as negligible. The Pareto charts confirmed the predominance of T_{mould}, which had by far the largest effect on the replication indicators. The second biggest effect was the second-order interaction between p_{hold} and T_{mould}: it was observed

that moulding with the high level of T_{mould} increased the effect of p_{hold}, making the setting of 750 bar more significant for achieving a better replication. The interaction between p_{hold} and v_{inj} was also significant, since only when using the high level of injection speed, was the increase of holding pressure beneficial for the replication. This happened because, when using a higher v_{inj}, a more efficient packing phase was possible thanks to the faster injection and consequently postponed freezing of the gate.

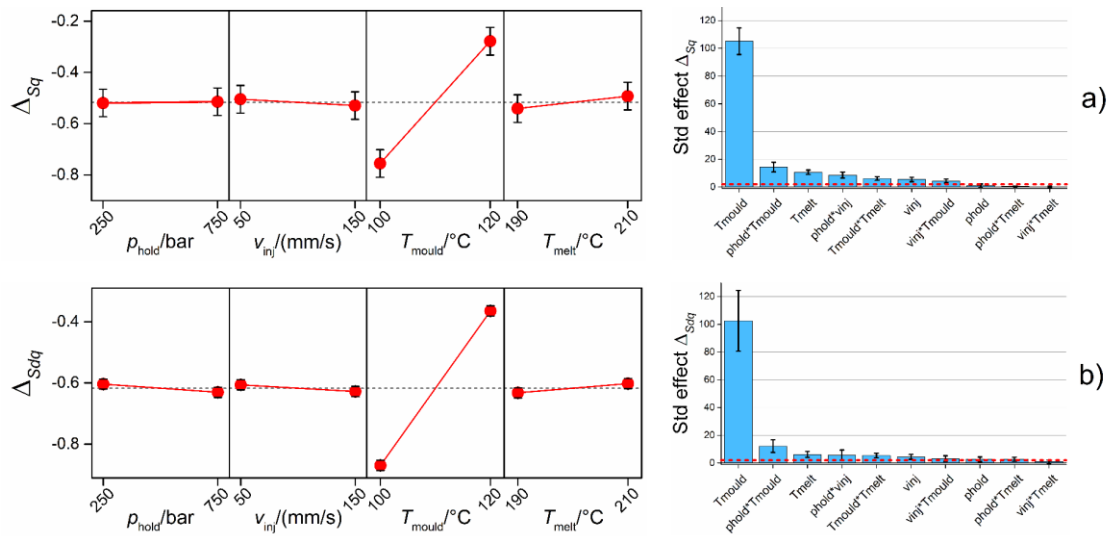

Fig. 12. Main effects plot (left) and Pareto chart of effects (right) for replication indicators a) Δ_{Sq} and b) Δ_{Sdq} for POM. Interval bars represent expanded measurement uncertainty U in the main effect plots and standard deviations of the effects due to the five DoE replicates in the Pareto charts. The red dashed line in the Pareto chart represents the significance limit at 95 % of confidence level.

Fig. 13 shows the results of the DoE analysis for PC. Similarly to the other material, the factor having the biggest impact on the replication was the mould temperature: setting a T_{mould} of 120 °C increased Δ_{Sq} and Δ_{Sdq} of 0.2 and 0.1 respectively, resulting in better-replicated nano ripples (see Table 6). As for POM, the effects of the other process parameters were covered by the measurement uncertainty and thus negligible with respect to the replication of height and slope of the laser-machined ripples. The Pareto chart shows that, as for POM, the second-order interactions between p_{hold} and T_{mould} and between p_{hold} and v_{inj} were significant.

When comparing the results for the two materials, it can be observed that the slopes of the main effects plots were the same for all the four investigated process variables considering both *Sq* and *Sdq* replication indicators. This proved that, even though the structure of the two polymers was different, µIM settings had the same impact on the replication of nano structures. However, the replication fidelity achieved when moulding POM was higher than that obtained with PC. This was particularly true when using the high level of mould temperature (see Table 6): if, on

one hand, POM was capable of replicating the master nano structures well when setting T_{mould} at 120 °C, on the other, PC only showed a slight improve with respect to the low setting condition. This was due to the fact that, at high shear rates, the selected POM has a slightly lower viscosity than PC (see Fig. 4 a)), resulting in a better overall replication of the master surface. Another potential cause for this discrepancy might be the different creep deformation behaviour of the two materials. Creep deformation has been reported in literature as a primary variable with respect to the replication of small features [38]: in the packing stage of the moulding cycle, the frozen skin layer undergoes a deformation that enhances the replication of surface features beyond the level reached during the initial filling. This phenomenon is strongly dependent on mould temperature and material properties. Being the T_{mould} settings closer to the flow temperature for POM than for PC (as also mirrored by the 100 °C higher melt temperature employed for the latter), it is probable that the solidified skin layer was softer for the first if compared to the second, particularly at T_{mould} equal to 120 °C. Therefore, the creep deformation contribution to surface replication was much more relevant for POM, which, in fact, exhibited a substantial increase of Δ_{Sq} and Δ_{Sdq}, as opposed to PC that showed a limited replication improvement.

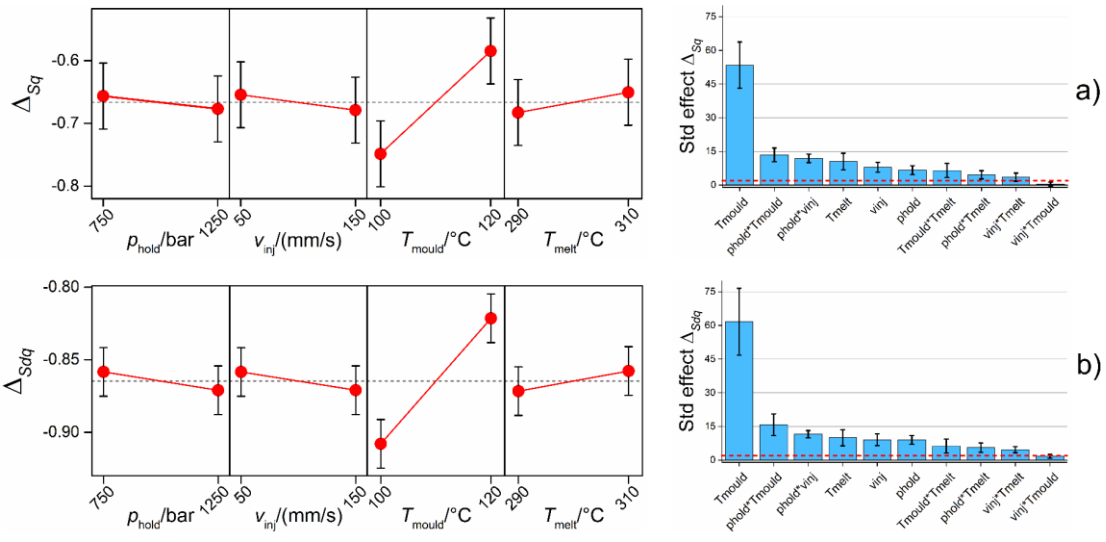

Fig. 13. Main effects plot (left) and Pareto chart of effects (right) for replication indicators a) Δ_{Sq} and b) Δ_{Sdq} for PC. Interval bars represent expanded measurement uncertainty U in the main effect plots and standard deviations of the effects due to the five DoE replicates in the Pareto charts. The red dashed line in the Pareto chart represents the significance limit at 95 % of confidence level.

Table 6 Surface replication at low and high T_{mould} for POM and PC as compared with the tool insert surface.

Tool insert	
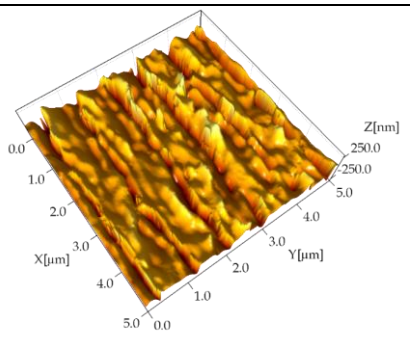	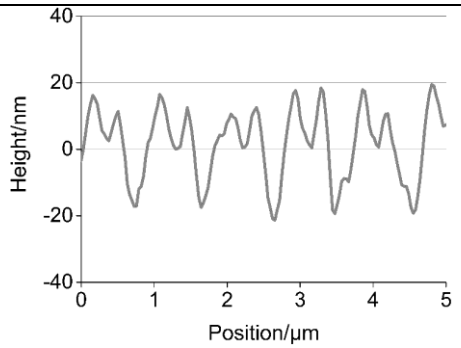
POM, T_{mould} = 100 °C	
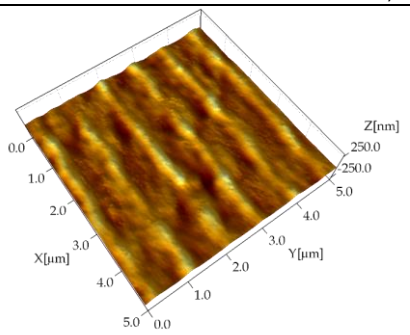	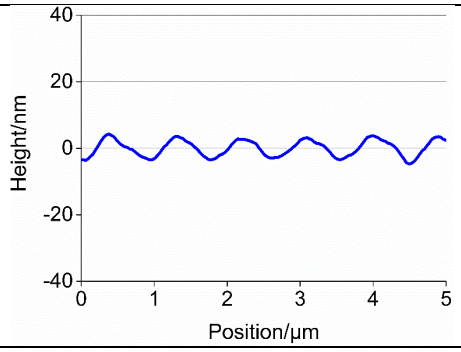
POM, T_{mould} = 120 °C	
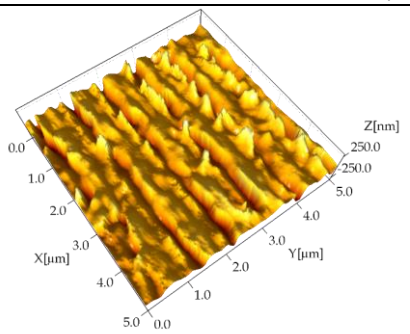	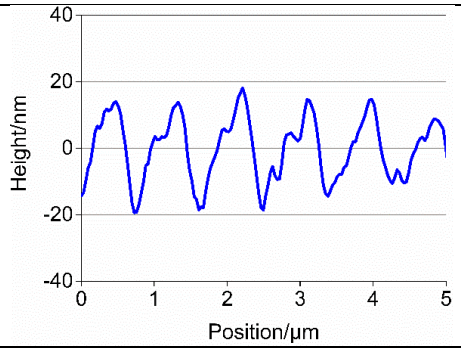
PC, T_{mould} = 100 °C	
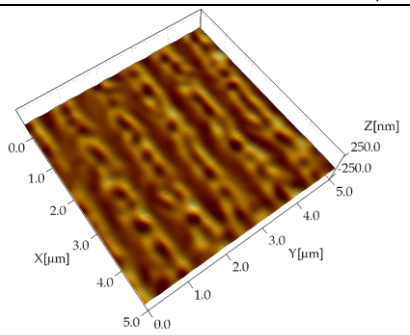	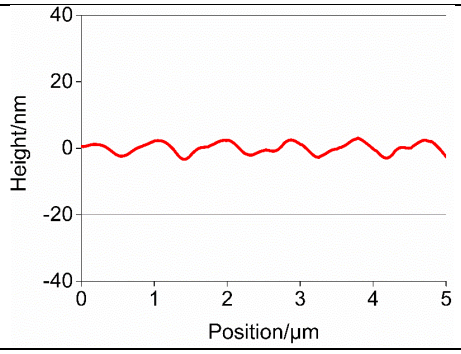
PC, T_{mould} = 120 °C	

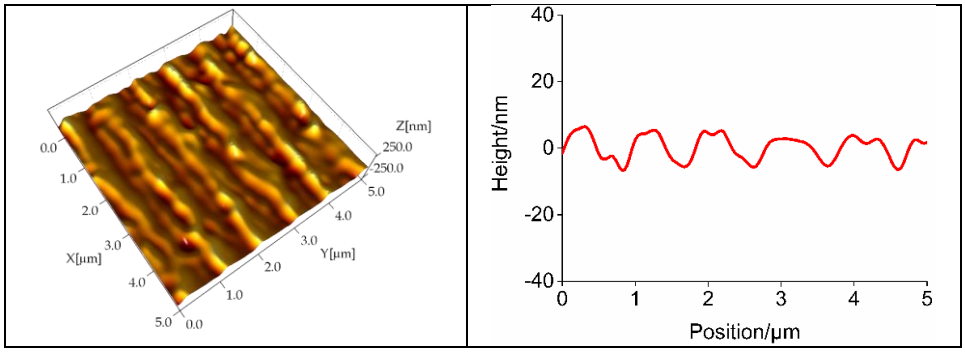

For both materials, Δ_{Sq} and Δ_{Sdq} values were correlated, as shown by the similar main effects plots and Pareto charts. The connection between the two indicators was due to the link between *Sq* and *Sdq*: when considering surfaces having similar characteristics, as those obtained replicating the same master geometry, an increase of average height comes with an increase of average slope and vice versa. This is clearly shown in Table 6: surfaces replicated with high T_{mould} have both increased height and slope with respect to those moulded with low T_{mould}. However, the correlation between Δ_{Sq} and Δ_{Sdq} is different for POM and PC. Fig. 14 shows the relationship between Δ_{Sq} and Δ_{Sdq} for the two materials described by a linear fit. It can be observed that the slope of the line fitting POM data is much higher than that of PC, meaning that an increase of Δ_{Sq} resulted in a smaller variation of Δ_{Sdq} for the latter. The reason for this must be searched in the peculiar morphology of the nano ripples, which have a complex shape on their upper part, with two peaks appearing for the majority of the cases (see Fig. 15 a)). This morphology was generated by the laser structuring process and was partially replicated only on the parts moulded with POM at high mould temperature (see Fig. 15 b)). In fact, the PC was not fully able to develop the double-peaked structure of the master, even when setting high T_{mould}. Having the two peaks a high slope, their presence in the profile influences more the value of *Sdq* than that of *Sq*. Therefore, while Δ_{Sq} was related to the capability of replicating the master surface with respect to the height, Δ_{Sdq} was linked on how well the peculiar morphology of the master nano ripples was reproduced on the replica. The increase of T_{mould} from 100 °C to 120 °C allowed POM to increase the replication of both height (mirrored by an increase of Δ_{Sq}) and morphology (mirrored by an increase of Δ_{Sdq}) of the master surface. Conversely, for PC only the replication of the height was improved significantly when setting high T_{mould}, since Δ_{Sdq} did not show a relevant increase, proving the double-peaked shape of the nano ripples was still not replicated. This analysis proved how the combined use of *Sq* and *Sdq* was necessary to

quantitatively characterize the difference between the different types of replication obtained with the two materials.

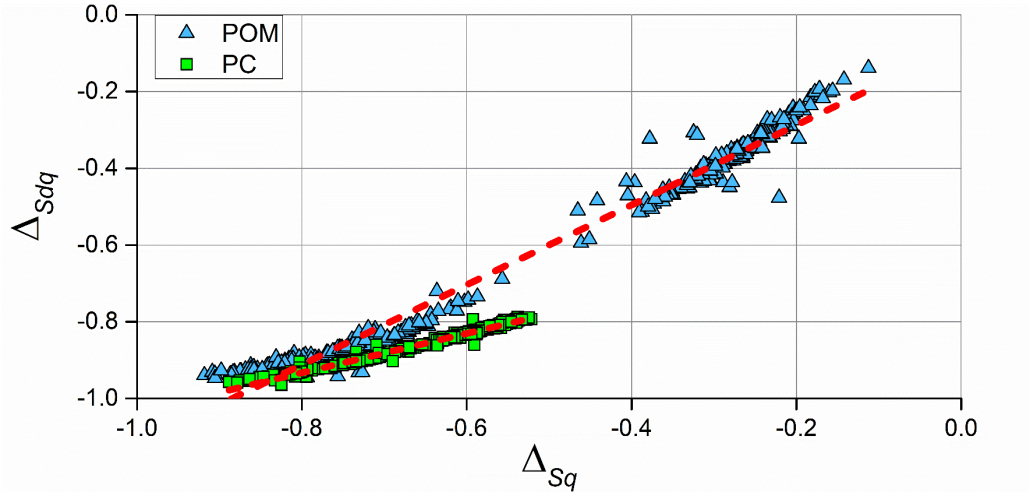

Fig. 14. Relationship between Δ_{Sq} and Δ_{Sdq} for the two moulded materials. Red dashed lines represent the fitted linear trend.

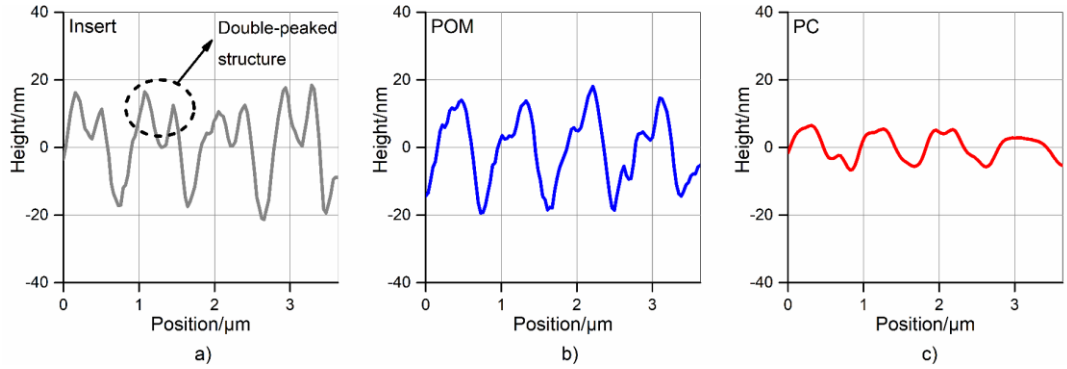

Fig. 15. Details of replicated structures. a) Nano ripples on the insert, b) on the replicated POM and c) on the replicated PC using the high T_{mould}. The shape of the upper part of the structures is highlighted.

3.2 Analysis of the monitored variables

3.2.1 Effect of holding pressure, injection speed and mould temperature

The effects of holding pressure, injection speed and mould temperature on the five variables extracted from the monitored temperature curves were investigated. This type of analysis is important since an effective fingerprint must be sensible to the variations of µIM process settings in order to be used as a tool for optimization.

Fig. 16 shows the main effects plots of the recorded variables for POM. T_{peak1} was positively influenced by v_{inj} and T_{mould}, while p_{hold} effect was negligible. This is linked to the burning phenomenon that generates the first temperature peak. In particular, a polymer melt having

higher speed generates a higher compression on the air in the cavity, thus enhancing T_{peak1}. The same effect was caused by an increase of mould temperature, meaning that a hotter cavity favoured the burning effect. Also, T_{peak2}, which is related to the maximum flow front temperature, increased when setting the high levels of v_{inj} and T_{mould}. A higher injection speed generates higher shear rates in the polymer melt and therefore a higher temperature due to shear heating. The effect of the mould temperature can be explained by considering that a larger amount of heat provided by the mould walls contributed to increasing melt flow temperature. The two average temperature T_{mean1} and T_{mean2} calculated in different time intervals (see Fig. 10) showed similar dependences on the process parameters. In particular, T_{mould} had the most important impact, resulting in an increase in both indicators when selecting its high level. This happened because selecting the high mould temperature both increased the initial plateau, which is correlated to T_{mean1}, and the second peak of temperature, which is correlated to T_{mean2}. The injection speed was significant only for T_{mean2}, while the holding pressure was negligible for both average temperatures.

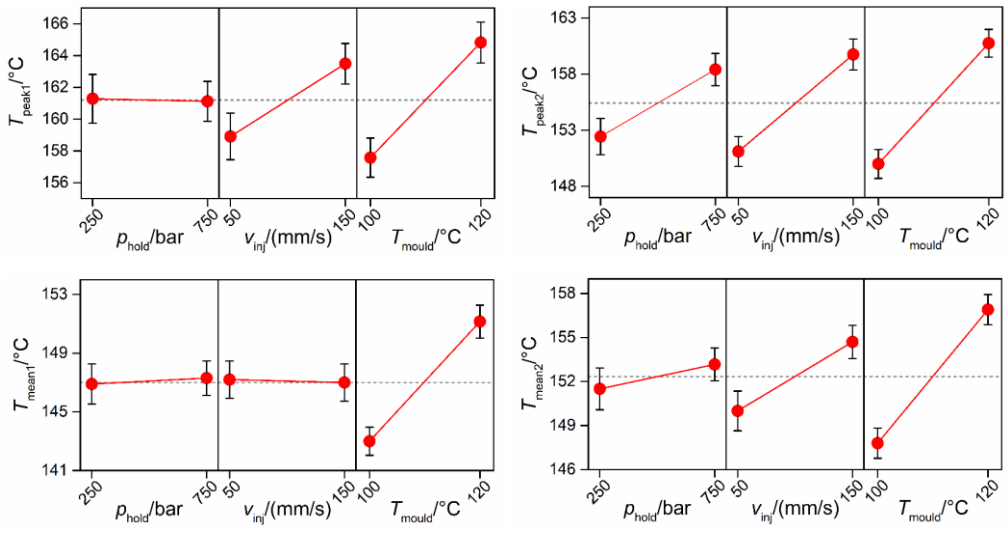

Fig. 16. Main effects plots of the four fingerprint candidates for POM. The interval bars represent standard errors for the specific level of the process parameter.

Fig. 17 shows the effects of the process parameters on the PC. Although the signs of the slopes are very similar to those of POM, thus confirming the physical explanations behind the effects, there are major differences in terms of the impact of the µIM process parameters on the fingerprint candidates. In fact, the injection speed had a much larger effect on T_{peak1}, T_{peak2} and T_{mean2} for PC if compared to POM, where the mould temperature played the most important role. This might have been due to the different molecular structure of the two materials: the

predominance of v_{inj} for PC suggests that the thermal history of this material was governed by the shear rate, which is strictly dependent on the injection speed. On the other hand, for POM, the temperature to which the melt was exposed in the cavity was the most important characteristics, being the mould temperature the parameter having the largest impact on most of the monitored indicators. The only indicator that was most dependent on T_{mould} for both POM and PC was T_{mean1} because of the fact that the initial plateau was equal to the mould temperature for both polymers.

Finally, it can be concluded that T_{peak1}, T_{peak2}, T_{mean1} and T_{mean2} were all sensible to the variation of process settings. In particular, they all showed a degree of dependence on T_{mould}, which was the parameter having the most relevant impact on the replication of the nano ripples (see Fig. 12 and Fig. 13), even though the dependence was greater for POM.

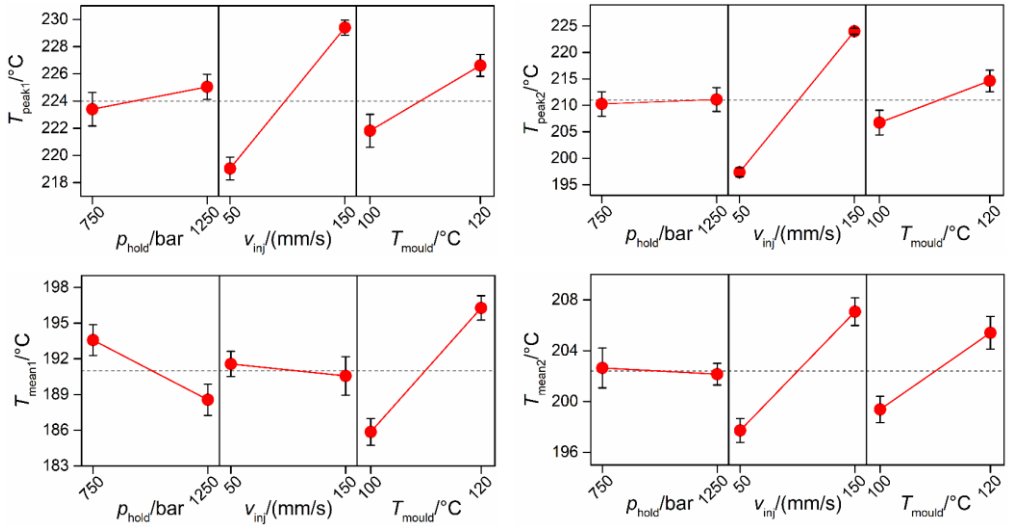

Fig. 17. Main effects plots of the four fingerprint candidates for PC. The interval bars represent standard errors for the specific level of the process parameter.

3.2.2 Effect of melt temperature

Fig. 18 graphically shows the effect of the melt temperature variation on the temperature profile and, as a consequence, on the process fingerprint candidates. It can be observed that increasing T_{melt} shifted the maximum temperature profile upwards, resulting in overall higher temperature because a polymer melt having higher thermal energy entered the cavity. As regards the process fingerprint candidates, both T_{peak1} and T_{peak2} increased their value when setting the high T_{melt}. In particular, the first temperature peak increased more than the second one, meaning that the burning effect was highly influenced by the initial polymer melt

temperature. In addition, T_{mean1} and T_{mean2} were also positively dependent on the melt temperature value because of the general rise of the T_{max} profile.

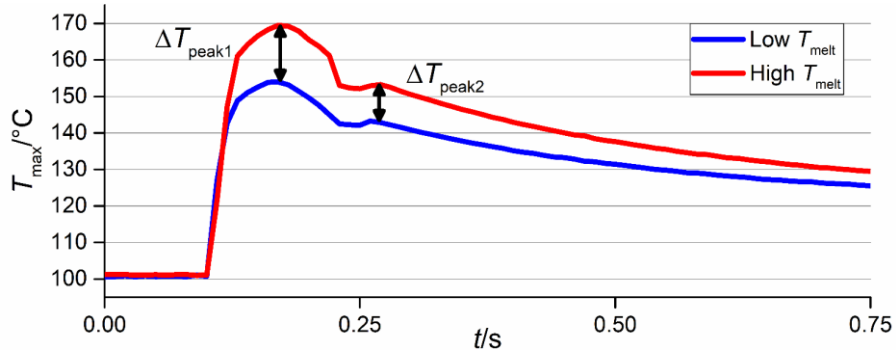

Fig. 18. Maximum temperature profiles when setting low (blue) and high (red) melt temperature with POM. The other process parameters were kept as fixed.

3.3 Process fingerprint identification

In order to identify the best process fingerprint, a correlation analysis was performed between replication quality and the five candidates extracted from cavity temperature profiles. In particular, the Pearson coefficient of correlation ρ was selected as an indicator of the level of correlation [40]. It is defined as:

$$\rho(\mathbf{x},\mathbf{y}) = \frac{\sum (x-\bar{x})(y-\bar{y})}{\sqrt{\sum (x-\bar{x})^2 \sum (y-\bar{y})^2}} \quad (4)$$

where **x** and **y** are two different datasets and $\bar{x}$ and $\bar{y}$ are their respective average values. ρ can assume values between -1 and +1, where the first corresponds to a perfect linear negative correlation, while the second to a perfect linear positive correlation. When ρ is equal to 0, no correlation among the two datasets exists.

Fig. 19 shows the coefficients of correlation calculated between the two replication indicators Δ_{Sq} and Δ_{Sdq} and the five process fingerprint candidates for both the moulded materials. In general, it can be seen that Δ_{Sq} and Δ_{Sdq} were very similarly correlated to the candidates, confirming the link between the two replication indicators (see Fig. 14). This is important since it proved how the replication in height and morphology of the nano ripples can be controlled using the same monitored variable.

As regard POM, ρ values close to 0.8 were observed for T_{peak1}, T_{mean1} and T_{mean2}, meaning that an increase of these variables happened with an improvement of the replication. The large correlation can also be seen by comparing the effects of µIM process parameters (see Fig. 12 and Fig. 16): for both replication indicators and these three fingerprint candidates, the mould temperature was the most relevant process setting. T_{peak2} showed a slightly lower correlation (ρ equal to circa 0.6).

The correlation pattern was different for PC. In general, an inferior level of correlation was observed, since, for all process fingerprint candidates, lower ρ values were calculated. In particular, only T_{mean1} showed a significant level of correlation (ρ equal to 0.75) with Δ_{Sq} and Δ_{Sdq}. The different behaviour of PC was caused by the fact that T_{mean1} was the only candidate for which the mould temperature played the most relevant role: the injection speed was, in fact, the most impactful process parameters for T_{peak1}, T_{peak2} and T_{mean2} (see Fig. 17). This discrepancy between the two materials regarding the correlation pattern could be caused by their different properties. In fact, as mentioned before, creep deformation played a more important role for POM than for PC because of the softer skin layer. Being the creep deformation strongly affected by the temperature at the mould-polymer interface, where the skin layer itself is formed, POM replication was generally more sensitive to temperature variations recorded with the high-speed infrared camera, of which the process fingerprint candidates are indicators. Therefore, a generally higher recorded temperature profile (i.e. higher process fingerprint candidate values) was probably linked to a more pronounced creep deformation of the skin layer for POM and, in turn, to a replication improvement. Oppositely, PC showed a less relevant correlation because the creep deformation played a lesser role in its replication mechanism within the explored experimental conditions.

In conclusion, the correlation analysis on the two materials proved that T_{mean1} was the best process fingerprint candidate, being process sensitive and the most correlated to the replication of the nano-structured surface. These finding demonstrated how the initial rise of temperature during the filling of the cavity (see Fig. 10) linked to the burning effect played an important role in determining the outcome of the moulding process.

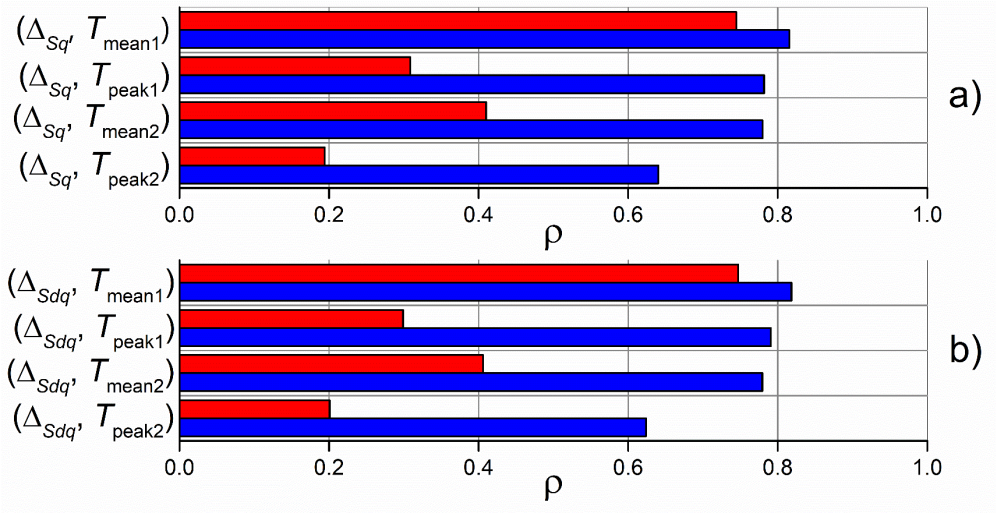

Fig. 19. Coefficients of correlation calculated between a) Δ_{Sq} and b) Δ_{Sdq} and the process fingerprint candidates for POM (blue) and PC (red).

Fig. 20 shows the replication indicators plotted against the selected process fingerprint T_{mean1} for both POM and PC. The relationship between the data is clear in both cases. For POM, two distinct subgroups of data are visible, corresponding to the parts moulded at low and high mould temperature. T_{mean1} is capable of describing this behaviour for both Δ_{Sq} and Δ_{Sdq}, which, as shown before, are highly correlated and look as just shifted along the y-axis. The relationship between the variables is positive since a higher value of the fingerprint came with an increase in the replication performance. This agrees with the slopes of the main effects plots (see Fig. 12 and Fig. 16) and the correlation coefficients that were, in fact, positive (see Fig. 19). Although there exist some dispersion around the depicted linear trend, it is clear that a T_{mean1} higher than 148 °C was of primary importance to maximize the replication of the nano-structured ripples. For PC, the performance of T_{mean1} in predicting the quality of the moulded surfaces was similar, since a clear positive trend existed among the data. In this case, however, there was not a distinct differentiation of Δ_{Sq} and Δ_{Sdq} in two subgroups, since the improvement in replication was less important. Therefore, direct recommendation on the value of the process fingerprint cannot be made as for POM. The plot also shows that the discrepancy between Δ_{Sq} and Δ_{Sdq} was higher for PC, particularly at their maxima, confirming that POM acted better in replicating both height and morphology of the nano structures. It can be concluded that, for both materials, controlling the value of T_{mean1} in-line allows to accurately control the replication of the nano-structured surface. Moreover, since T_{mean1} was calculated based on the first part of the maximum temperature profile (see Fig. 10), only the initial phase of the moulding cycle has to

be recorded, thus lowering the computational burden for an actual in-line quality assurance process. By applying this approach, a substantial improvement with respect to the random assessment of produced samples can be achieved. In fact, by checking the process fingerprint value at each cycle, accurate information on the surface replication can be gathered without the need of performing lengthy surface topography measurements that also require the samples to be transferred to a metrological laboratory. The usefulness of the method is maximized in the process optimization phase, where wide ranges of process parameters have to be explored and, therefore, many experiments have to be carried out. Moreover, this approach directly allows the evaluation of process repeatability, whereas the randomic assessment is based only on few samples and, as such, might not describe how well the process outputs are repeated in time.

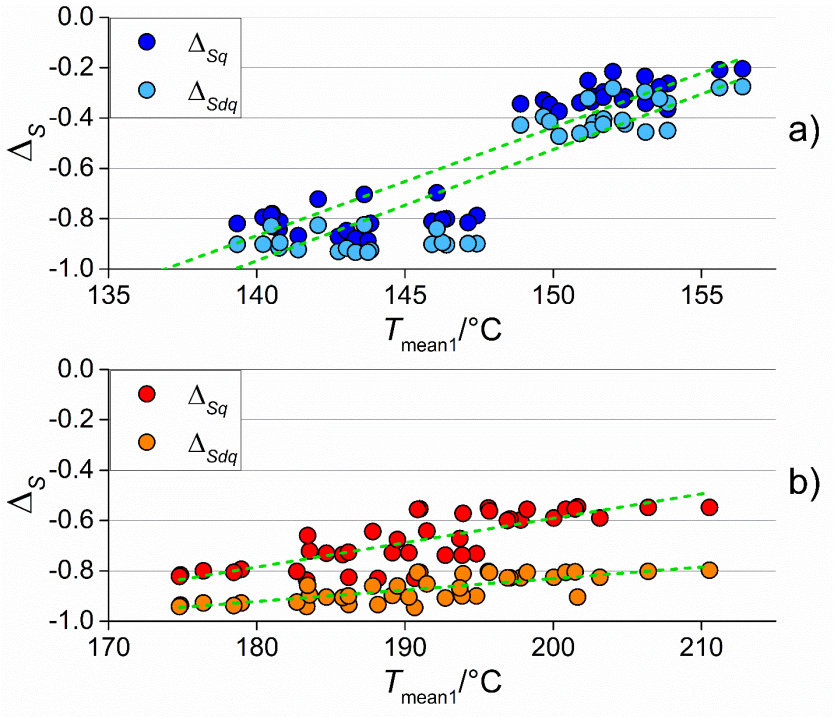

Fig. 20. Replication indicators versus T_{mean1} for a) POM and b) PC. Red dashed lines represent the linear trends.

4. Conclusions

The present paper investigated the applicability of a novel in-line monitoring concept for the surface replication of nano structures by µIM using two polymers having a different molecular structure, POM and PC. The monitored variables were extracted from acquisitions performed with a high-speed infrared camera that imaged the cavity through a sapphire window. The

produced surfaces were characterized using a laser confocal scanning microscope and the replication quality was successfully correlated to a selected monitored variable, opening the door to fast and accurate control of surface replication in µIM.

The following conclusions can be drawn from the study:

- The use of the infrared camera allowed a useful visualization of the melt flow inside the cavity as well as the extraction of the thermal history of the polymer.
- For both materials, the effects of the variations of the investigated µIM process parameters on the replication quality were similar, making the observed trend more general given the different molecular structure of POM and PC.
- The mould temperature was the most impactful process parameters for the replication of the nano ripples. In particular, setting its high level significantly improved the replicated features using both POM and PC.
- The combined use of replication indicators based on the areal roughness parameters *Sq* and *Sdq* allowed characterizing the main difference in terms or replication for the two materials. If, on one hand, POM was capable of well reproducing the nano ripples in terms of both height and morphology, on the other, PC was not accurate in replicating the morphology of the nano structures. The different replication performance of the two materials was most probably caused by a combination of the slightly lower viscosity of and more pronounced creep deformation of POM at high T_{mould}.
- The indicators extracted from the temperature profiles acquired with the infrared camera were most dependent on the mould temperature and the injection speed. In particular, T_{mould} was the most significant parameter for POM, while v_{inj} had a bigger impact on PC.
- The correlation analysis revealed that the mean temperature during the initial rise T_{mean1} was the one most correlated with the replication quality, demonstrating how the initial phase of the filling played a primary role with respect to the output of the µIM process.
- Using T_{mean1} as a process fingerprint seemed very promising since it showed a clear relationship with the replication quality for both the moulded materials, proving that the process can be effectively controlled by checking the value of a variable monitored during the moulding cycle. For POM, in particular, a threshold value for obtaining high-quality parts could be set at circa 148 °C.

Acknowledgements

This research work was undertaken in the context of MICROMAN project ("Process Fingerprint for Zero-defect Net-shape MICROMANufacturing", http://www.microman.mek.dtu.dk/). MICROMAN is a European Training Network supported by Horizon 2020, the EU Framework Programme for Research and Innovation (Project ID: 674801). This research has also received funding from the European Union's Horizon 2020 research and innovation programme under grant agreement No. 766871 (HIMALAIA). The project H2020 ITN Laser4Fun (agreement No. 675063) is also acknowledged.

References

[1] Attia UM, Marson S, Alcock JR. Micro-injection moulding of polymer microfluidic devices. Microfluid Nanofluidics 2009;7:1–28. doi:10.1007/s10404-009-0421-x.

[2] Huang C, Li L, Yi AY. Design and fabrication of a micro Alvarez lens array with a variable focal length. Microsyst Technol 2009;15:559–63. doi:10.1007/s00542-008-0706-0.

[3] Hansen HN, Hocken RJ, Tosello G. Replication of micro and nano surface geometries. CIRP Ann - Manuf Technol 2011;60:695–714. doi:10.1016/j.cirp.2011.05.008.

[4] Giboz J, Copponnex T, Mélé P. Microinjection molding of thermoplastic polymers: a review. J Micromechanics Microengineering 2007;17:R96–109. doi:10.1088/0960-1317/17/6/R02.

[5] Metwally K, Barriere T, Khan-Malek C. Replication of micrometric and sub-micrometric structured surfaces using micro-injection and micro-injection compression moulding. Int J Adv Manuf Technol 2016;83:779–89. doi:10.1007/s00170-015-7602-4.

[6] La M, Lee JG, Park SJ. Numerical and experimental investigation of plastic injection molding of micro-engineered surfaces. Polym Eng Sci 2017;51:E73–81. doi:10.1002/pen.24652.

[7] Vella PC, Dimov SS, Brousseau E, Whiteside BR. A new process chain for producing bulk metallic glass replication masters with micro- and nano-scale features. Int J Adv Manuf Technol 2014;76:523–43. doi:10.1007/s00170-014-6148-1.

[8] Lucchetta G, Sorgato M, Carmignato S, Savio E. Investigating the technological limits of micro-injection molding in replicating high aspect ratio micro-structured surfaces. CIRP Ann - Manuf Technol 2014;63:521–4. doi:10.1016/j.cirp.2014.03.049.

[9] Masato D, Sorgato M, Lucchetta G. Analysis of the influence of part thickness on the replication of micro-structured surfaces by injection molding. Mater Des 2016;95:219–24. doi:10.1016/j.matdes.2016.01.115.

[10] Tosello G, Gava A, Hansen HN, Lucchetta G. Study of process parameters effect on the filling phase of micro-

injection moulding using weld lines as flow markers. Int J Adv Manuf Technol 2010;47:81–97. doi:10.1007/s00170-009-2100-1.

[11] Vera J, Brulez A-C, Contraires E, Larochette M, Trannoy-Orban N, Pignon M, et al. Factors influencing microinjection molding replication quality. J Micromechanics Microengineering 2018;28:015004. doi:10.1088/1361-6439/aa9a4e.

[12] Speranza V, Liparoti S, Calaon M, Tosello G, Pantani R, Titomanlio G. Replication of micro and nano-features on iPP by injection molding with fast cavity surface temperature evolution. Mater Des 2017;133:559–69. doi:10.1016/j.matdes.2017.08.016.

[13] Kuhn S, Burr A, Kübler M, Deckert M, Bleesen C. Study on the replication quality of micro-structures in the injection molding process with dynamical tool tempering systems. Microsyst Technol 2010;16:1787–801. doi:10.1007/s00542-010-1104-y.

[14] Baruffi F, Calaon M, Tosello G. Effects of micro-injection moulding process parameters on accuracy and precision of thermoplastic elastomer micro rings. Precis Eng 2018;51:353–61. doi:10.1016/j.precisioneng.2017.09.006.

[15] Calaon M, Tosello G, Garnaes J, Hansen HN. Injection and injection-compression moulding replication capability for the production of polymer lab-on-a-chip with nano structures. J Micromechanics Microengineering 2017;27. doi:10.1088/1361-6439/aa853f.

[16] Sorgato M, Masato D, Lucchetta G. Effect of vacuum venting and mold wettability on the replication of micro-structured surfaces. Microsyst Technol 2016;23:2543–52. doi:10.1007/s00542-016-3038-5.

[17] Hansen HN, Carneiro K, Haitjema H, De Chiffre L. Dimensional micro and nano metrology. CIRP Ann - Manuf Technol 2006;55:721–43. doi:10.1016/j.cirp.2006.10.005.

[18] Madsen JS, Thamdrup LH, Czolkos I, Hansen PE, Johansson A, Garnaes J, et al. In-line characterization of nanostructured mass-produced polymer components using scatterometry. J Micromechanics Microengineering 2017;27:085004. doi:10.1088/1361-6439/aa7a3a.

[19] Baruffi F, Calaon M, Tosello G. Micro-injection moulding in-line quality assurance based on product and process fingerprints. Micromachines 2018;9. doi:10.3390/mi9060293.

[20] Griffiths CA, Dimov S, Scholz SG, Hirshy H, Tosello G. Process Factors Influence on Cavity Pressure Behavior in Microinjection Moulding. J Manuf Sci Eng 2011;133:031007. doi:10.1115/1.4003953.

[21] Lucchetta G, Masato D, Sorgato M, Crema L, Savio E. Effects of different mould coatings on polymer filling flow in thin-wall injection moulding. CIRP Ann - Manuf Technol 2016;65:537–40. doi:10.1016/j.cirp.2016.04.006.

[22] Su Q, Gilchrist MD. Demolding forces for micron sized features during micro-injection molding. Polym Eng Sci 2016;56:810–6. doi:10.1002/pen.24309.

[23] Zhang N, Chu JS, Byrne CJ, Browne DJ, Gilchrist MD. Replication of micro/nano-scale features by micro injection molding with a bulk metallic glass mold insert. J Micromechanics Microengineering 2012;22. doi:10.1088/0960-1317/22/6/065019.

[24] Whiteside B, Martyn MT, Coates PD, Allan PS, Hornsby PR, Greenway G. Micromoulding: process characteristics and product properties. Plast Rubber Compos 2003;32:231–9.

[25] Tosello G, Hansen HN. Micro-injection-molding. Micro-Manufacturing Eng Technol 2010:90–113. doi:10.1016/B978-0-8155-1545-6.00006-5.

[26] Han X, Yokoi H. Visualization analysis of the filling behavior of melt into microscale V-grooves during the filling stage of injection molding. Polym Eng Sci 2006;46:1590–7. doi:10.1002/pen.20615.

[27] Sorgato M, Babenko M, Lucchetta G, Whiteside B. Investigation of the influence of vacuum venting on mould surface temperature in micro injection moulding. Int J Adv Manuf Technol 2017;88:547–55. doi:10.1007/s00170-016-8789-8.

[28] Babenko M, Sweeney J, Petkov P, Lacan F, Bigot S, Whiteside B. Evaluation of heat transfer at the cavity-polymer interface in microinjection moulding based on experimental and simulation study. Appl Therm Eng 2018;130:865–76. doi:10.1016/j.applthermaleng.2017.11.022.

[29] Guerrier P, Tosello G, Nielsen KK, Hattel JH. Three-dimensional numerical modeling of an induction heated injection molding tool with flow visualization. Int J Adv Manuf Technol 2016;85:643–60. doi:10.1007/s00170-015-7955-8.

[30] Surace R, Bellantone V, Trotta G, Fassi I. Replicating capability investigation of micro features in injection moulding process. J Manuf Process 2017;28:351–61. doi:10.1016/j.jmapro.2017.07.004.

[31] ISO 16610-61: Geometrical product specification (GPS) - Filtration - Part 61: Linear areal filters - Gaussian filters 2015.

[32] ISO 25178-2: Geometrical product specifications (GPS) - Surface texture: Areal - Part 2: Terms, definitions and surface texture parameters 2012.

[33] Lutey AHA, Gemini L, Romoli L, Lazzini G, Fuso F, Faucon M, et al. Towards laser-textured antibacterial surfaces. Sci Rep 2018;8:1–10. doi:10.1038/s41598-018-28454-2.

[34] Bagherifard S, Hickey DJ, de Luca AC, Malheiro VN, Markaki AE, Guagliano M, et al. The influence of nanostructured features on bacterial adhesion and bone cell functions on severely shot peened 316L stainless steel. Biomaterials 2015;73:185–97. doi:10.1016/j.biomaterials.2015.09.019.

[35] Hasan J, Crawford RJ, Ivanova EP. Antibacterial surfaces: The quest for a new generation of biomaterials. Trends Biotechnol 2013;31:295–304. doi:10.1016/j.tibtech.2013.01.017.

[36] ISO 15530 -3: Geometrical product specifications (GPS) - Coordinate measuring machines (CMM): Technique

for determining the uncertainty of measurement 2011.

[37] Tosello G, Haitjema H, Leach RK, Quagliotti D, Gasparin S, Hansen HN. An international comparison of surface texture parameters quantification on polymer artefacts using optical instruments. CIRP Ann - Manuf Technol 2016;65:529–32. doi:10.1016/j.cirp.2016.04.003.

[38] Zhang H, Fang F, Gilchrist MD, Zhang N. Filling of high aspect ratio micro features of a microfluidic flow cytometer chip using micro injection moulding. J Micromechanics Microengineering 2018;28. doi:10.1088/1361-6439/aab7bf.

[39] Sha B, Dimov S, Griffiths C, Packianather MS. Investigation of micro-injection moulding: Factors affecting the replication quality. J Mater Process Technol 2007;183:284–96. doi:10.1016/j.jmatprotec.2006.10.019.

[40] James F. Statistical Methods In Experimental Physics. 2nd ed. Singapore: World Scientific; 2006.